The Kinematic Effects of the Defects in Liquid Crystal Dynamics

Rui Chen[1], Weizhu Bao[2] and Hui Zhang[3,*]

[1] *Institute of Applied Physics and Computational Mathematics, Beijing 100088, P.R. China.*
[2] *Department of Mathematics, National University of Singapore, Singapore, 119076.*
[3] *School of Mathematical Sciences, Beijing Normal University, Laboratory of Mathematics and Complex Systems, Ministry of Education, Beijing 100875, P.R. China.*

Abstract. Here we investigate the kinematic transports of the defects in the nematic liquid crystal system by numerical experiments. The model is a shear flow case of the viscoelastic continuum model simplified from the Ericksen-Leslie system. The numerical experiments are carried out by using a difference method. Based on these numerical experiments we find some interesting and important relationships between the kinematic transports and the characteristics of the flow. We present the development and interaction of the defects. These results are partly consistent with the observation from the experiments. Thus this scheme illustrates, to some extent, the kinematic effects of the defects.

AMS subject classifications: 65M70, 76A15

Key words: Nematic liquid crystals, kinematic effects, finite difference method, defects.

1 Introduction

The molecules of nematic liquid crystals have long-range orientational order and can be easily aligned by external forces. This will result in defects, textures and other important phenomena, e.g. disclination [4, 6, 10, 13, 32]. Many efforts have been made on theories to explore the liquid dynamics, such as Ericksen-Leslie (EL) theory [8, 10], tensor models [1, 24, 25], hard-rod models [6, 10, 12], capillary models [28, 30, 33, 34] and so on. Recently, many mathematicians are absorbed in investigating the solutions of these theoretical models, including the numerical simulations [7, 9, 17, 19, 20, 22, 23, 26, 36, 37, 39–41] and theoretical analysis [16, 18, 21] and references therein.

Corresponding author. Email addresses: `ruichenbnu@gmail.com` (R. Chen), `bao@cz3.nus.edu.sg` (W. Z. Bao), `hzhang@bnu.edu.cn` (H. Zhang)

Defects are classified in terms of strength (S) and dimensionality (D). The strength captures the degree of rotational discontinuity when encircling the defect, whereas the dimension refers to points ($D=0$), lines ($D=1$) and walls ($D=2$) [13,14,27]. Disclinations are line defects with $D=1$ and disclination ends cannot be found in the bulk. The strength of a disclination line is defined by a sign $(+,-)$ and a magnitude $(1/2,1,3/2,2,\cdots)$. The sign indicates the direction of rotation and the magnitude is the amount of rotation. The defects with $s=\pm1/2$ or $s=\pm1$ has a singular core.

Toch et al. [35], showed that back-flow, the coupling between the order parameter and the velocity fields, has a significant effect on the motion of defects in nematic liquid crystals. In particular the defect speed can depend strongly on the topological strength in two dimensions and on the sense of rotation of the director about the core in three dimensions. They also considered that the annihilation of a pair of defects of strength $s=\pm1/2$ and found that back-flow can change the speed of defects by up to $\sim100\%$. Rey et al. [11,29,31] investigated the interaction of defects with different strength and compared them with the experiments. Here we study the interaction of defects immersing the fluids and find some interesting and important relationships between the kinematic transports and the characteristics of the flow.

In the Ericksen-Leslie (EL) theory, a vector field **d** is used to depict the alignment of the molecules and also to represent the direction of preferred orientation of the molecules in the neighbourhood of any point. The evolution of **d** expresses the kinematic motions. By the Ericksen and Leslie theory, the model is derived as the following nonlinear coupled system for nematic liquid crystals in fluid field [19,21]:

$$\mathbf{u}_t+(\mathbf{u}\cdot\nabla)\mathbf{u}+\nabla p=\mu\triangle\mathbf{u}+\lambda\nabla\cdot\sigma, \tag{1.1}$$

$$\nabla\cdot\mathbf{u}=0, \tag{1.2}$$

$$\sigma=(\nabla\mathbf{d})^T\nabla\mathbf{d}+\beta(\triangle\mathbf{d}-\mathbf{f}(\mathbf{d}))\mathbf{d}^T+(\beta+1)\mathbf{d}(\triangle\mathbf{d}-\mathbf{f}(\mathbf{d}))^T, \tag{1.3}$$

$$\mathbf{d}_t+(\mathbf{u}\cdot\nabla)\mathbf{d}+D_\beta(\mathbf{u})\mathbf{d}=\gamma(\triangle\mathbf{d}-\mathbf{f}(\mathbf{d})). \tag{1.4}$$

Here **u** denotes the velocity of the nematic liquid crystals fluid, p the pressure, **d** the orientation of the molecules, $\mathbf{u},\mathbf{d}:\Omega\times\mathbb{R}^+\rightarrow\mathbb{R}^3, p:\Omega\times\mathbb{R}^+\rightarrow\mathbb{R}, \Omega\subset\mathbb{R}^2$. $\mathbf{x}\in\Omega$ is the Eulerian coordinate. μ,λ and γ are positive constants. In Eq.(1.4) $\mathbf{f}(\mathbf{d})=(4/\varepsilon^2)(|\mathbf{d}|^2-1)\mathbf{d}$ can be treated as a penalty function to approximate the constraint $|\mathbf{d}|=1$ which is due to the molecules being of similar size for small ε. The corresponding energy density is $F(\mathbf{d})=(1/\varepsilon^2)(|\mathbf{d}|^2-1)^2$ and it is obvious $\mathbf{f}(\mathbf{d})$ is the gradient of $\nabla F(\mathbf{d})$. We define $D_\beta(\mathbf{u})=\beta\nabla\mathbf{u}+(1+\beta)(\nabla\mathbf{u})^T$ for $\beta\in\mathbb{R}$. Hence, it can be rewritten as

$$D_\beta(\mathbf{u})=-\frac{\nabla\mathbf{u}-(\nabla\mathbf{u})^T}{2}-(-2\beta-1)\frac{\nabla\mathbf{u}+(\nabla\mathbf{u})^T}{2}. \tag{1.5}$$

The parameter β depends on the shape of the molecules. In Eq. (1.4), the kinematic transport of **d** is $\frac{D}{Dt}\mathbf{d}=\mathbf{d}_t+(\mathbf{u}\cdot\nabla)\mathbf{d}+D_\beta(\mathbf{u})\mathbf{d}$. When the size of the molecules is small compared with the scale of the macroscopic fluid, **d** is just transported by the flow trajectory. Then the kinematic transport of **d** is $\frac{D}{Dt}\mathbf{d}=\mathbf{d}_t+(\mathbf{u}\cdot\nabla)\mathbf{d}$ without the effect term $D_\beta(\mathbf{u})\mathbf{d}$ of

stretch on **d** [16–18,20,22,23]. When the size of the molecules are big enough, the effect of stretch on **d** must be taken into account. In the big molecule case, the parameter relating to the shape of molecules is important. In the original EL theory, this parameter is called *tumbling parameter*. Effect of different values of tumbling parameter and Ericksen number on spatial development of director orientation in pressure-driven channel flow was investigated by Chono et al. in [3]. The parameter $-2\beta-1$ in Eq. (1.5) is called the *reactive parameter*, or *tumbling parameter* in EL theory [15]. For nematic LC composed of rod-like molecules, we have $\beta < -0.5$ while for those composed of disc-like molecules, $\beta > -0.5$. In [19,20] β is confined within the interval $[-1,0]$. Actually β can take any real value and the nematic LC is *tumbling* as $|2\beta+1|<1$ while it is *flow-aligning* as $|2\beta+1|>1$ [11,28]. This is due to the fact that β also depends on the second and fourth moments of the distribution of molecules about the nematic director and this dependence can not be predicted by EL theory itself. When the nematic LC is flow-aligning, it has steady state in a simple shear flow, and there will be a flow-aligning angle related to β.

From the viewpoint of mathematician, the disclination lines and defects are singular solutions. For the above system with the suitable boundary condition we can verify it to satisfy some energy relation. So the physical singularities we are seeking/tracking are those energetically admissible ones. A C^0 finite element scheme is used to simulate the kinematic effects in [19]. A number of hydrodynamical liquid crystal examples were computed to demonstrate the effects of the parameters and the performance of the method. Later we developed the modified Crank-Nicolson finite difference scheme for the planar pressure driven flow where the direction of the molecules is constrained in the shear plane. This scheme satisfies a discrete energy relation in [40]. It is observed numerically that the direction of the molecules will tumble from the boundary layer and later on the inner layer with a much longer time period. It implies that the viscosity of flow plays the role of an accelerator in the whole complex fluids. Comparing these results with the theoretical analysis, it illustrates that the gradient of the velocity has directly impact on the tumbling phenomena. In [41], we applied an accurate and efficient Legendre-Galerkin method to investigate the effects of kinematic transports by numerical experiments and some theoretical analysis. The scheme also keeps the energy relation in discrete form. Consequently, for the system with steady state solutions, the number of spatial rotations is determined by the shape parameter of molecules β and the shear rate of the initial data. Theoretical analysis was made to explain the results. Moreover, in [41], the authors verified the relationship between the tumbling period and two important parameters for the tumbling flow. Flow-aligning nematic LCs were also concerned.

Now we will investigate numerically the kinematic effects of the defects in nematic liquid crystal dynamics for the simplified three dimensional flow case. Here a finite difference method in 2D Eulerian space was designed to approximate the simplified 3D model more specifically. We adopt a semi-implicit scheme which is implicit on linear terms and explicit on nonlinear terms. The scheme is high efficient although it does not preserve discrete energy relation. We also obtain similar numerical results comparing with the ones solved by the scheme preserving the discrete energy relation. Here

we present a number of examples that show the dynamics and interaction of defects with different strength. The numerical tests imply that the defects subjected to strength $|s|=1$ are stable and the system will be developed into a new stable defects with strength $s'(=\Sigma_{i=1}^{N}s_i)$ as the initial defects with strength s_i $(i=1,\cdots,N)$ are given. These phenomena were observed in [4,10] for 2D case. Here we show that there also exist this law in simple 3D case. Especially, we can see the fact that the annihilation time of the opposite defects is longer as the shear rate of back-flow is larger, when the four defects with $s=1$ distribute isometrically around a center defect with $s=-1$. We hope this phenomena happen in physical experiment in the future. But it is regretted that we have not found the experiment results for 3D case. Therefore, This implies that the model from the Ericksen-Leslie theory can also describe the kinematic effect of the defects.

This paper is organized as follows. We first introduce the simple case of the full model in Section 2 and derive the semi-implicit scheme of finite difference method in Section 3. Then in Section 4 numerical tests and discussions are given. Finally, we draw some conclusions and remarks.

2 Model for the simple case

In this section, we first show the energy relation for the full model with certain boundary conditions (B.C.). Then we will give the simple case of Eqs. (1.1)-(1.4) with the initial value and boundary condition.

Here we will investigate the system (1.1)-(1.4) with the following B.C. of **u**

$$\mathbf{u}\cdot\mathbf{n}=0, \quad \frac{\partial\mathbf{u}}{\partial\mathbf{n}}=\mathbf{g_u}, \quad \text{on } \partial\Omega, \tag{2.1}$$

where **n** denotes the outer normal vector on the boundary and $\mathbf{g_u}$ is a given vector. These mean that there is a rotation flow on the boundary. In the following we can see that this may push the liquid crystal particles to produce defects.

For the direction of **d**, the Robin boundary condition is used as follows

$$\frac{\partial\mathbf{d}}{\partial\mathbf{n}}=-\frac{2}{\delta}(\mathbf{d}-\mathbf{d}^0), \quad \text{on } \partial\Omega. \tag{2.2}$$

Actually under this choice of B.C., one term called anchoring energy is added into the total energy. The parameter $\delta>0$ reflects the strength of the anchoring. We believe that this is more reasonable than fixing **d** on the boundary. Because this Robin B.C. means the balance between the anchoring force and the other external force on the boundary. In this sense we say it is better than the strong anchoring condition. In the following simple model, the B.C. (2.8) and (2.9) satisfy the above B.C. (2.1) and (2.2). In [41], Zhang et al. has proved that the system (1.1)-(1.4) with (2.1) and (2.2) satisfies the following energy

relation [41]

$$\frac{d}{dt}\left(\frac{1}{2}||\mathbf{u}||^2_{L^2(\Omega)}+\frac{\lambda}{2}||\nabla\mathbf{d}||^2_{L^2(\Omega)}+\lambda\int_\Omega F(\mathbf{d})dx+\frac{\lambda}{\delta}\int_{\partial\Omega}|\mathbf{d}-\mathbf{d}_0|^2dS\right)$$

$$=-\left(\mu||\nabla\mathbf{u}||^2_{L^2(\Omega)}+\frac{\lambda}{\gamma}||\mathbf{d}_t+(\mathbf{u}\cdot\nabla\mathbf{d})\mathbf{d}+D_\beta(\mathbf{u})\mathbf{d}||^2_{L^2(\Omega)}\right)$$

$$+\int_{\partial\Omega}(\mathbf{g_u}\cdot\mathbf{u})dS+\int_{\partial\Omega}(\sigma_1:\mathbf{u}\otimes\mathbf{n})dS, \tag{2.3}$$

where $\sigma_1=\beta(\Delta\mathbf{d}-\mathbf{f}(\mathbf{d}))\mathbf{d}^T+(\beta+1)\mathbf{d}(\Delta\mathbf{d}-\mathbf{f}(\mathbf{d}))^T$. The energy relation plays an important role in both theoretical analysis [21] and numerical simulation [19,40]. We will derive the energy function in the discrete form from the energy relation (2.3) in Section 3.

Next we will present the main role in this work which is a simple case of the above full system. Now we also use a simplified 3D model, assuming that $\mathbf{u}=(0,v(z,x),0)^T$, $p=p(z,x)$, $\mathbf{d}=(0,d_2(z,x),d_3(z,x))^T$, $(z,x)\in\Omega=[-1,1]\times[-1,1]$ as shown in Fig. 1. It is obvious to see that there are two variables z,x in this model. In fact, it is the simple three dimensional case since the full 3D model is very difficult. Here we choose the initial value $v^0(z,x)=\xi z$, ξ is a constant to be the shear velocity which depends on z and is independent of x.

From Fig. 1 we can see that the direction $\mathbf{d}(z,x)$ is in the y-z plane. Here we can see that it looks like a "rice field" of the (x,z) plane. And $\mathbf{d}$ is a piece of rice growing on this field. In order to plot and view the direction $\mathbf{d}$ of every point in the z-x plane conveniently, we can change the order of $\mathbf{d}$ as $\hat{\mathbf{d}}=(d_2(z,x),0,d_3(z,x))^T$. For this shear flow case, the full model can be simplified as follows

$$v_t=\mu\triangle v+\lambda\tau_z, \tag{2.4}$$

$$\tau=\beta d_3(\triangle d_2-f_2)+(\beta+1)d_2(\triangle d_3-f_3), \tag{2.5}$$

$$d_{2t}+\beta d_3 v_z=\gamma(\triangle d_2-f_2), \tag{2.6}$$

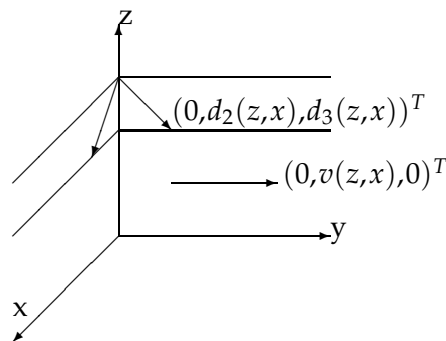$$d_{3t}+(1+\beta)d_2 v_z=\gamma(\triangle d_3-f_3), \tag{2.7}$$

Figure 1: "1+2" model, "1" denotes one component v of the velocity $\mathbf{u}$, and "2" denotes two components of the director $\mathbf{d}$.

where $f_i = (4/\varepsilon^2)(d_2^2 + d_3^2 - 1)d_i$, $v^0 = \xi z, d_2^0, d_3^0$ and the boundary conditions:

$$\frac{\partial v}{\partial z}\Big|_{z=\pm 1} = \xi, \quad \frac{\partial v}{\partial x}\Big|_{x=\pm 1} = 0, \tag{2.8}$$

$$\frac{\partial d_i}{\partial \mathbf{n}} = -\frac{2}{\delta}(d_i - d_i^0), \quad i = 2,3 \quad \text{on } \partial\Omega. \tag{2.9}$$

The parameters included in this system are $\mu, \lambda, \gamma, \varepsilon$ and β, ξ. In Section 4 we will discuss the impact of the shape parameter β of molecular and the shear rate ξ.

3   Numerical method

This section mainly focuses on the numerical approximation. In order to obtain the high efficient computation, we choose difference schemes comparing with the method in [19]. For the space discretization we adopt the semi-implicit scheme and use the forward difference scheme for the time discretization:

$$\frac{d_{2j,i}^{n+1} - d_{2j,i}^n}{dt} + \beta d_{3ji}^n \frac{\delta_{0z}v_{j,i}^n}{2h} = \gamma\left(\frac{\delta_z^2 d_{2j,i}^{n+1} + \delta_x^2 d_{2j,i}^{n+1}}{h^2} - f_{2j,i}^n\right), \tag{3.1}$$

$$\frac{d_{3j,i}^{n+1} - d_{3j,i}^n}{dt} + (1+\beta)d_{2j,i}^n \frac{\delta_{0z}v_{j,i}^n}{2h} = \gamma\left(\frac{\delta_z^2 d_{3j,i}^{n+1} + \delta_x^2 d_{3j,i}^{n+1}}{h^2} - f_{3j,i}^n\right), \tag{3.2}$$

$$\tau_{j,i}^n = \beta d_{3j,i}^n \frac{1}{\gamma}\left(\frac{d_{2j,i}^{n+1} - d_{2j,i}^n}{dt} + \beta d_{3j,i}^n \frac{\delta_{0z}v_{j,i}^n}{2h}\right)$$

$$+ (\beta+1)d_{2j,i}^n \frac{1}{\gamma}\left(\frac{d_{3j,i}^{n+1} - d_{3j,i}^n}{dt} + (1+\beta)d_{2j,i}^n \frac{\delta_{0z}v_{j,i}^n}{2h}\right), \tag{3.3}$$

$$\frac{v_{j,i}^{n+1} - v_{j,i}^n}{dt} = \mu\left(\frac{\delta_z^2 v_{j,i}^{n+1} + \delta_x^2 v_{j,i}^{n+1}}{h^2}\right) + \lambda\frac{\delta_{0z}\tau_{ji}^n}{2h}, \tag{3.4}$$

where $\delta_{0z}v_{j,i}^n = v_{j,i+1}^n - v_{j,i-1}^n$, $\delta_z^2 d_{j,i} = d_{j,i+1} + d_{j,i-1} - 2d_{j,i}$, $\delta_x^2 d_{j,i} = d_{j+1,i} + d_{j-1,i} - 2d_{j,i}$, $f_{kj,i}^n = (4/\varepsilon^2)[(d_{2j,i}^n)^2 + (d_{3j,i}^n)^2 - 1]d_{kj,i}^n$, $k = 2,3$, $h = 2/M$. We discrete the domain Ω by $M \times M$ and we use a uniform grid. In Eq. (3.3) we have replaced $\gamma(\Delta\mathbf{d} - \mathbf{f}(\mathbf{d}))$ with $\mathbf{d}_t + (\mathbf{u}\cdot\nabla)\mathbf{d} + D_\beta(\mathbf{u})\mathbf{d}$ according to Eq. (1.4) to reduce the order of derivatives. The discretization of the boundary conditions are determined below

$$\frac{d_{kj,M}^{n+1} - d_{kj,M-1}^{n+1}}{h} = -\frac{2}{\delta}(d_{kj,M}^{n+1} - d_{kj,M}^0), \tag{3.5}$$

$$\frac{d_{kj,1}^{n+1} - d_{kj,0}^{n+1}}{h} = \frac{2}{\delta}(d_{kj,0}^{n+1} - d_{kj,0}^0), \tag{3.6}$$

$$\frac{d_{kM,i}^{n+1} - d_{kM-1,i}^{n+1}}{h} = -\frac{2}{\delta}(d_{kM,i}^{n+1} - d_{kM,i}^0), \tag{3.7}$$

$$\frac{d_{k1,i}^{n+1} - d_{k0,i}^{n+1}}{h} = \frac{2}{\delta}(d_{k0,i}^{n+1} - d_{k0,i}^0), \tag{3.8}$$

$$\frac{v_{j,M}^{n+1} - v_{j,M-1}^{n+1}}{h} = \xi, \quad \frac{v_{j,1}^{n+1} - v_{j,0}^{n+1}}{h} = \xi, \tag{3.9}$$

$$v_{M,i}^{n+1} = v_{M-1,i}^{n+1}, \quad v_{0,i}^{n+1} = v_{1,i}^{n+1}. \tag{3.10}$$

In [40] Zhang and Bai used the modified Crank-Nicolson scheme for preserving the discrete energy relation and dealt with the nonlinear terms with the fix point iteration. Now, the semi-implicit scheme we used is more efficient although it does not preserve discrete energy relation. After computing and comparing these two schemes we conclude that these two numerical results are similar. Thus we persist on adopting the semi-implicit scheme for high efficient computation. Later we define a discrete energy function corresponding the energy law in Eq. (2.3) as follows

$$E^n = \frac{1}{2}||v^n||_{L^2(\Omega)}^2 + \frac{\lambda}{2}\sum_{i=2,3}||\nabla d_i^n||_{L^2(\Omega)}^2$$

$$+ \lambda\int_\Omega F(d_2^n, d_3^n)dx + \frac{\lambda}{\delta}\left(\sum_{i=2,3}\int_{\partial\Omega}(d_i^n(x) - d_i^0(x))^2 dx\right), \tag{3.11}$$

where $F(d_2^n, d_3^n) = 1/(\varepsilon^2)(d_2^{n2} + d_3^{n2} - 1)^2$. We will calculate it to verify the stability of numerical solution in the following numerical simulations.

4   Numerical tests and discussion

In this section we will calculate a number of numerical examples to show the relation of the critical parameters and the kinematic effects of the defect. All the results are carried out with C++ and all the figures are drawn by MATLAB and TECPLOT.

4.1   Parameters

The relationship of the key parameters have been explored in our previous paper [41] for the simplest case with one variable. Here we concern with the case with two variables and choose the difference scheme instead of the spectral method in [41]. So we expect to verify again the relationship of the key parameters of the shear rate ξ and the shape parameter β. We set the mesh grid as $M \times M = 40 \times 40$ and the time step $dt = 1 \times 10^{-4}$. We mainly focus on the impact of β and ξ. The other parameters are set to be: $\gamma = 1$, $\mu = 1$, $\lambda = 1$, $\varepsilon = 0.1$, $\delta = 5 \times 10^{-5}$.

Set $\beta = -0.5$, $\xi = 10, 30, 40, 50$ and initial values to be

$$v^0(z,x) = \xi z, \quad d_2^0(z,x) = -1, \quad d_3^0(z,x) = 0, \quad (z,x) \in [-1,1] \times [-1,1]. \tag{4.1}$$
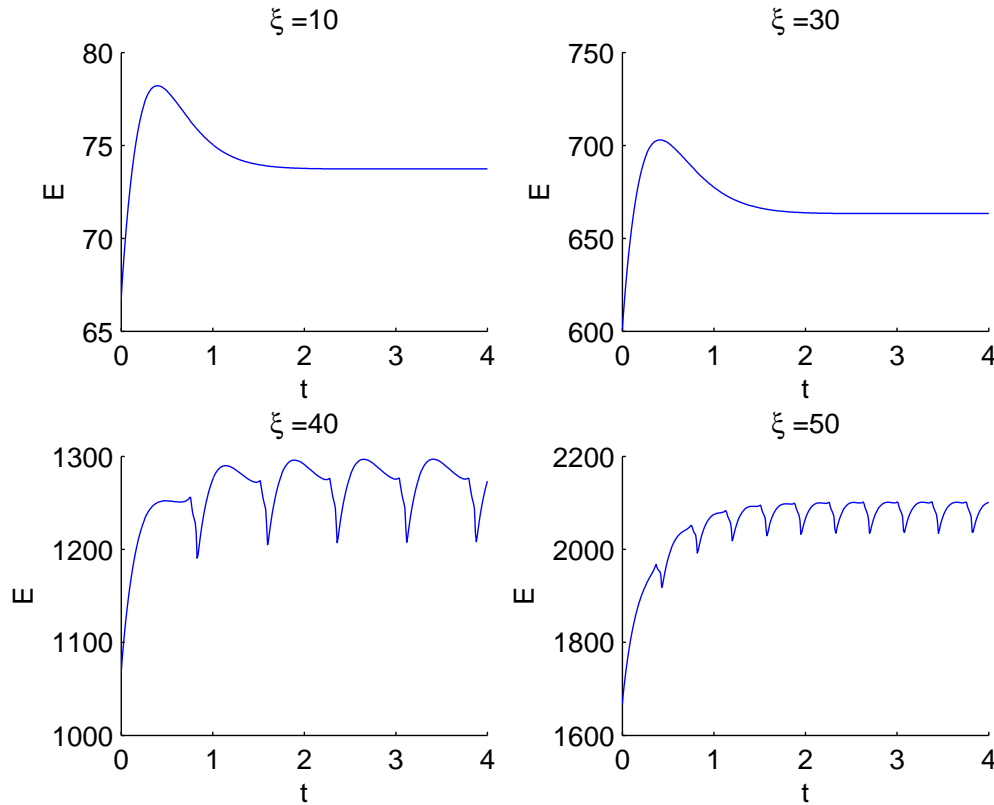
Figure 2: $\beta = -0.5$, energy function with different ξ.

The numerical result of the energy function Eq. (3.11) is given in Fig. 2. We can see that the system goes to steady state as $\xi = 10,30$ and periodic oscillation as $\xi = 40,50$. In fact, the steady state of the molecules is the tumbling found in [40,41] for $\xi = 40,50$. While the steady state is flow-aligning for $\xi = 10,30$ in [41]. This shows that there is competition of the force between the flow and the interaction among particles.

It also suggests us that the shear rate ξ cannot be chosen too large when we investigate the interaction of defect. A large shear rate will break the stability of system.

Now we investigate the impact on system with different β. We fix the shear rate $\xi = 30$ and the initial values are the same as Eq. (4.1). We compute the energy of the solutions for the different shape parameter $\beta = -0.1, -0.2, -0.3, -0.4, -0.6, -0.7, -0.8, -0.9$ respectively as shown in Fig. 3. In all the simulations the system go to steady states finally when ξ is fixed. Thus we can draw the conclusion that the steady state of the system only depends on the shear rate ξ while the total energy in steady states depends on both ξ and β. We can also see from Fig. 3 that the energy in steady states as $\beta \sim -1$ is smaller than that as $\beta \sim 0$. These results are consistent with the results in [41] by using the spectral method.
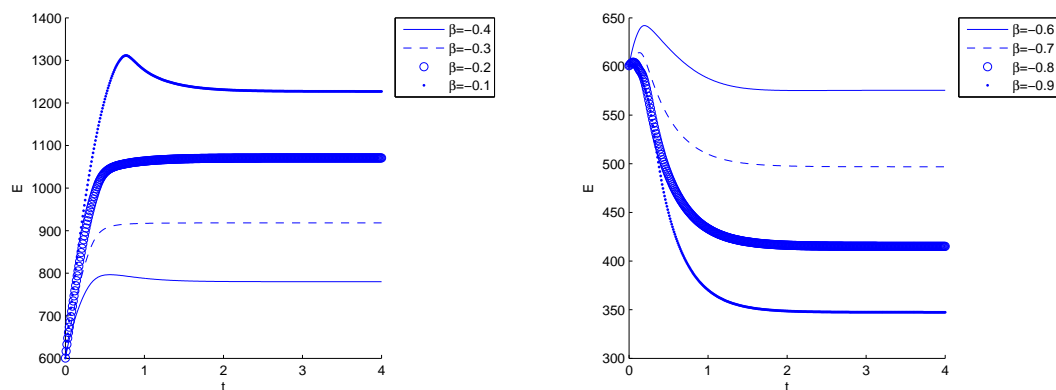
Figure 3: $\xi = 30$, energy function with different β.

4.2 Defects

In this section we will simulate the kinematic transport of the defects. The strength of a disclination is denoted by a parameter s as in [4,13]. Now we take the components of the unit director to be $(\cos\phi, \sin\phi)$, where the director angle ϕ is concerned with the polar angle α depicted in Fig. 4 satisfying the formula

$$\phi = s\alpha + c. \tag{4.2}$$

Here α is determined by director orientation along the polar line (x-axis) and ϕ is determined by director end along the polar line (x-axis) and c is a constant. The director is on the polar line as $s=1$, $c=0$ and on a circle as $s=1$, $c=\frac{\pi}{2}$. One can refer to [4,14] to find out the detail about the reason why s is the strength of defect. Now from the experiments there can be observed defects of strengths $s=+\frac{1}{2},-\frac{1}{2},+1,-1$ [4,10]. It is possible that two neighbouring defects annihilate altogether or form a new defect. The corresponding strength is $s_1+s_2=0$ or $s_1+s_2=s'$. Next we will simulate the kinematic transport of several defects with different strengths and we will show the interaction of the defects.
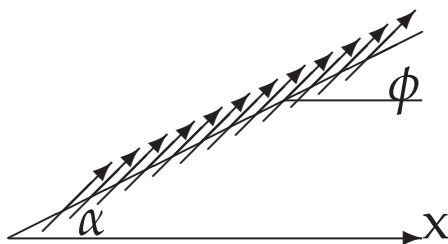
Figure 4: $\phi = s\alpha + c$.

Assume that N is the total number of defects and s_j denotes the strength of the jth defect and $X = (z,x) \in \Omega$ and $X_j^0 = (z_j^0, x_j^0)$ denotes the jth singular point. Now we define the complex function $g_{s_j}(X - X_j^0)$ similar to [2] as follows:

$$g_{s_j}(X - X_j^0) = \|X - X_j^0\|[\cos(\phi_j) + i\sin(\phi_j)] = \|X - X_j^0\|e^{i\phi_j}, \tag{4.3}$$
$$\phi_j = s_j\alpha_j + c, \tag{4.4}$$

where α_j is the argument of the vector $X - X_j^0$ and $\|X - X_j^0\|$ denotes the Eulerian distance from point X to X_0. Multiply all these complex functions

$$g_0(X) = \begin{cases} \displaystyle\prod_{j=1}^{N} \frac{g_{s_j}(X - X_j^0)}{\|X - X_j^0\|}, & X \in \Omega \setminus \{X_j^0, j = 1, \cdots, N\}, \\ 0, & X \in \{X_j^0, j = 1, \cdots, N\}, \end{cases} \tag{4.5}$$

thus we can get the initial value $d_2^0(X)$ and $d_3^0(X)$ from the complex function $g_0(X)$ as follows

$$d_2^0(X) = Im(g_0(X)), \quad d_3^0(X) = Re(g_0(X)). \tag{4.6}$$

In the following we will give a number of numerical examples to show the kinematic effects of the defect.

case 1:
(a) $N = 2$, $X_1^0 = (-0.2, 0)$, $X_2^0 = (0.2, 0)$, $s_1 = s_2 = 1$, $\xi = 3$;
(b) $N = 2$, $X_1^0 = (-0.85, 0)$, $X_2^0 = (0.85, 0)$, $s_1 = 1$, $s_2 = -1$, $\xi = 3$;

case 2:
(a) $N = 3$, $X_1^0 = (-0.2, 0)$, $X_2^0 = (0, 0)$, $X_3^0 = (0.2, 0)$, $s_1 = s_2 = s_3 = 1$, $\xi = 3$;
(b) $N = 3$, $X_1^0 = (-0.85, 0)$, $X_2^0 = (0, 0)$, $X_3^0 = (0.85, 0)$, $s_1 = s_3 = 1$, $s_2 = -1$, $\xi = 3$;

case 3:
(a) $N = 5$, $X_1^0 = (-0.2, 0)$, $X_2^0 = (0, 0.2)$, $X_3^0 = (0.2, 0)$, $X_4^0 = (0, -0.2)$, $X_0^0 = (0, 0)$, $s_0 = s_1 = s_2 = s_3 = s_4 = 1$, $\xi = 3$;
(b) $N = 5$, $X_1^0 = (-0.4, 0)$, $X_2^0 = (0, 0.4)$, $X_3^0 = (0.4, 0)$, $X_4^0 = (0, -0.4)$, $X_0^0 = (0, 0)$, $s_1 = s_2 = s_3 = s_4 = 1$, $s_0 = -1$, $\xi = 3$.

Here the parameter $\beta = -0.5$ is fixed in all the cases.

From Fig. 5 and Fig. 6, we know that two defects with the same strength $+1$ and $+1$ will repel each other and are rotating in the area. While the defects with $+1$ and -1 will attract each other until they annihilate. It happens between $t = 1.5$ to $t = 2$. This is consistent with result in [5]. We also see that both of the cases go to steady state. From Fig. 6 the energy will rapidly decrease when the defects with $+1$ and -1 collide.

From Figs. 7-8 we know that as time goes on, three defects of the same strength will repel until the system goes to steady state. We also find that the defect with $+1$ in the
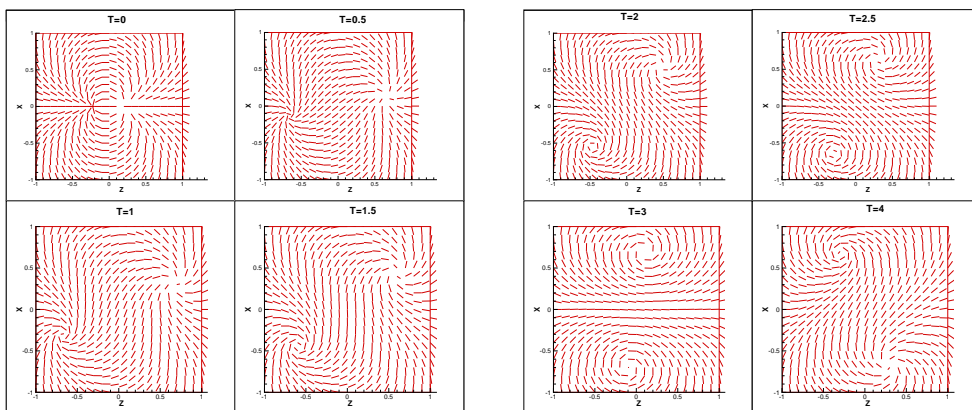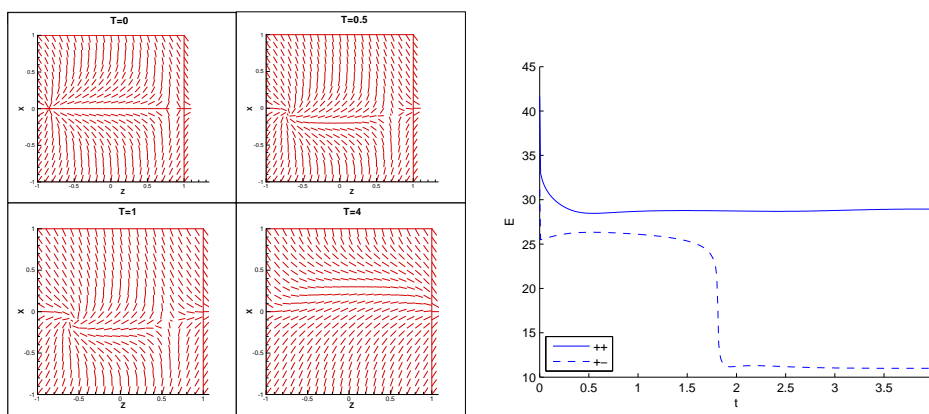
Figure 5: case1-(a).

Figure 6: Left: case1-(b); right: energy function.
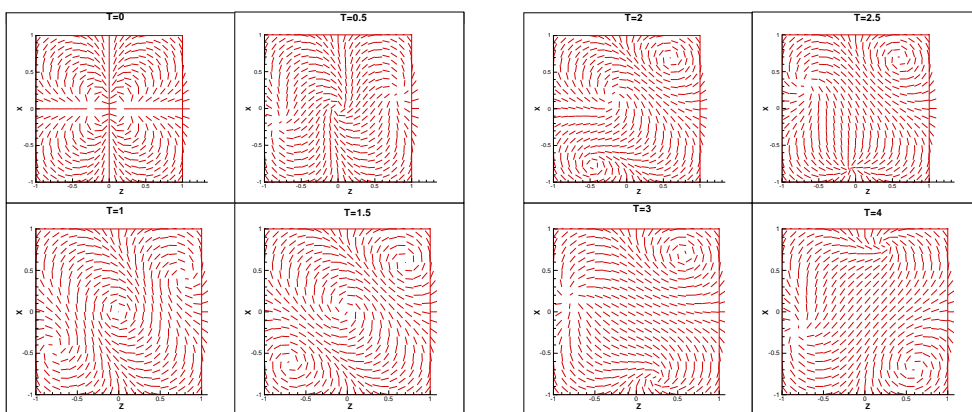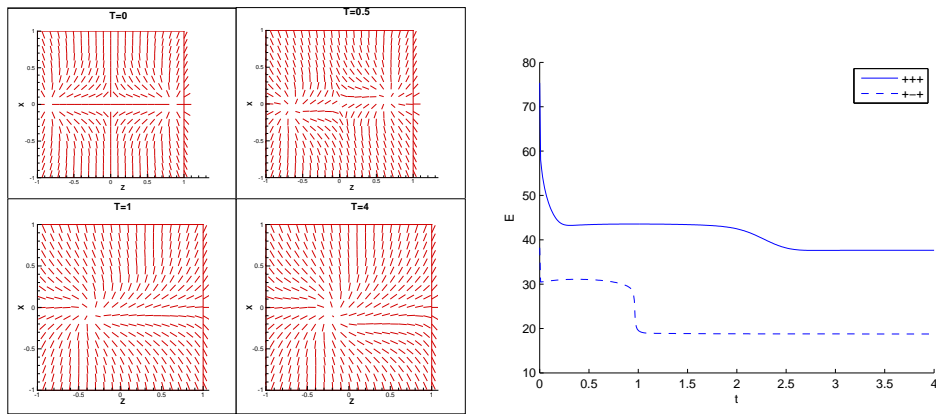

Figure 7: case2-(a).

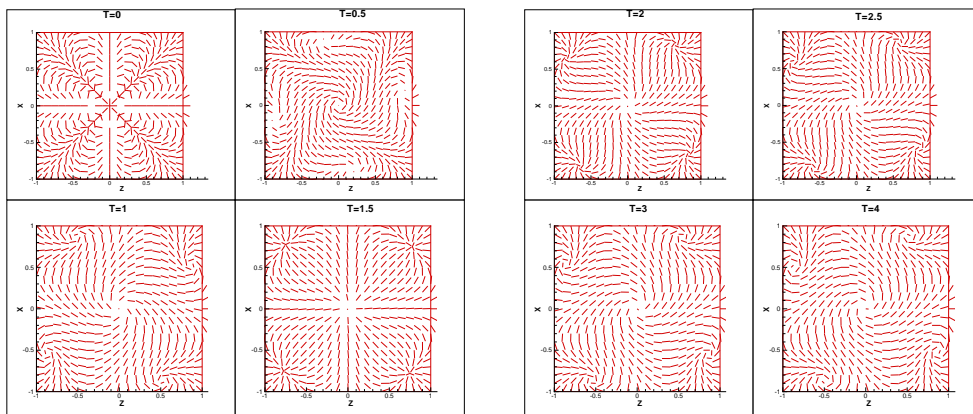Figure 8: Left: case2-(b); right: energy function.

Figure 9: case3-(a).

center of the region will move towards to the boundary of the region from Fig. 7. We can draw a conclusion that the energy of defects nearby the boundary is less than one in the center of the region by the energy function from Fig. 8. A defect with negative sign strength will attract one of the others positive defects, which occurs at the time $t=1$ in Fig. 8. The right part of Fig. 8 shows that the energy of case 2 ends with steady state.

In the case 3 the defects of the same strength repel each other and turn in the area from Fig. 9. Similarly, if the strength of the center defect is opposite to others and the other four defects are distributed symmetrically, the center defect with -1 will attract one of the remaining defects with $+1$ from Fig. 10, and annihilate at the time $t=3$. At last there are only three defects with strength $+1$. All the systems also go to steady state from Fig. 10. If we increase the shear rate $\xi=10,30,50$, we can see that the annihilation time is longer along the addition of ξ from the development of energy in Fig. 11. Here we see that the energy is oscillation for the large shear rate in Fig. 11, which is consistent with the result in Fig. 2 since there is tumbling.
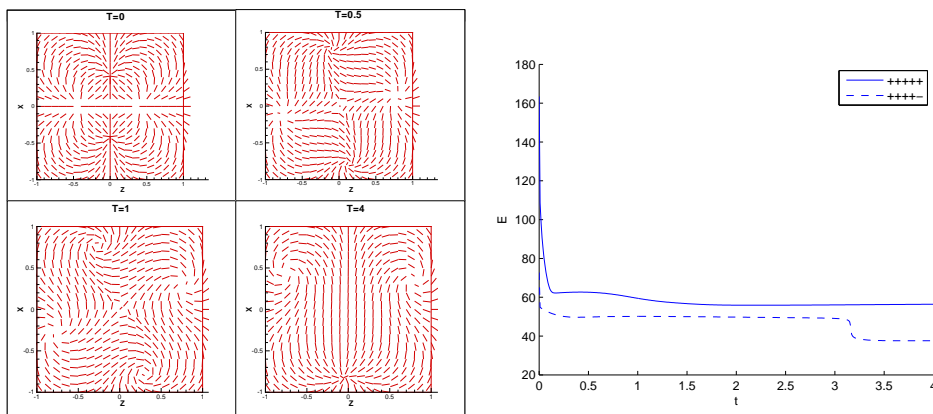
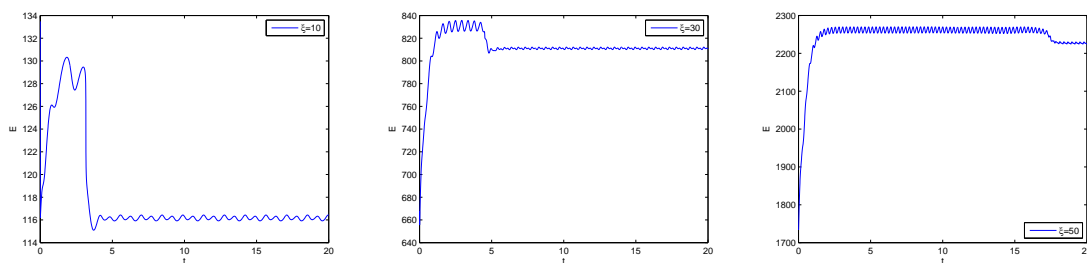Figure 10: Left: case3-(b); right: energy function.

Figure 11: case3-(b), left: $\tilde{\xi}=10$; middle: $\tilde{\xi}=30$; right: $\tilde{\xi}=50$.
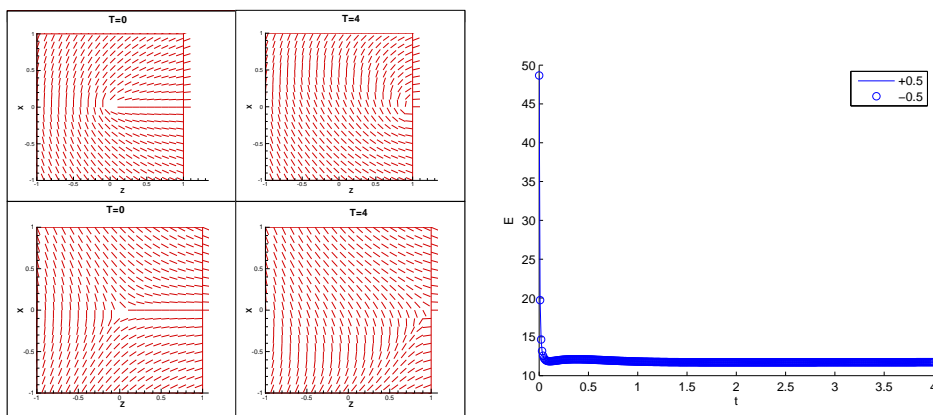

Figure 12: Left (up: $s=+\frac{1}{2}$; down: $s=-\frac{1}{2}$); right: energy function.

In the following we will simulate the defects with strength $s=\pm\frac{1}{2}$ and see how the defects interact in the system. From Fig. 12 we know that the defect of strength $|s|=\frac{1}{2}$ will move to the boundary of the area and then the system is stable.
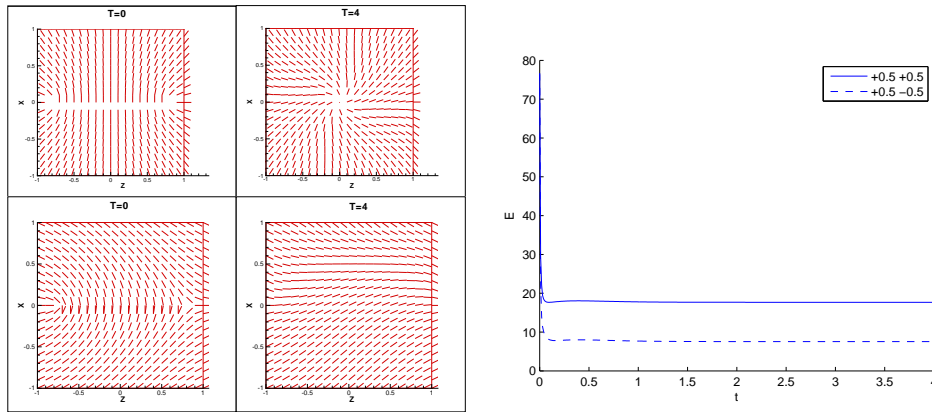
Figure 13: Left (up: $s_1 = s_2 = +\frac{1}{2}$; down: $s_1 = +\frac{1}{2}$, $s_2 = -\frac{1}{2}$); right: energy function.

From Fig. 13 we see that the defect with strength $s = +\frac{1}{2}$ will attract another defect with strength $s = +\frac{1}{2}$ to form a new defect of strength $s = +1$. While there will be no defect if one defect with strength $s = +\frac{1}{2}$ and the other defect with strength $s = -\frac{1}{2}$ are given at the beginning.

Remark 4.1. Here we also change the boundary condition of the vector **d** as the Dirichlet or Neumann boundary condition to test. It is found that there does not appear defect when the initial value has no defect. So the emergence of defect is not caused by the boundary condition in this case.

5   Conclusions and remarks

In this paper we applied the simplified three dimensional model to investigate the kinematic effect of the defect of the nematic liquid crystals fluid. A finite difference method is adopted to simulate the simplified model. We did some numerical tests to investigate the impact of the shape parameter β and the back-flow ξ. If the back-flow is strong, there is a tumbling of the molecular. Then we mainly did some numerical tests to explore the interaction of defects with different strength. The tests tell us that the strength of defects satisfies the law $\Sigma_{i=1}^{N} s_i = s'$ if there are many defects with different strength. Moreover, the interaction of these defects is not caused by the boundary conditions.

Acknowledgement

References

[1] D. W. Berrenman and S. Meiboom, Tensor representation of Oseen-Frank strain energy in uniaxial cholesterics, Phys. Rev. A, 30 (1984), 1955-1959.

[2] W. Z. Bao and Y. Z. Zhang, Dynamics of the ground state and central vortex states in Bose-Einstein condensation, M3AS, 15 (2005), 1863-1896.

[3] S. Chonoa, T. Tsujia and M. M. Denn, Spatial development of director orientation of tumbling nematic liquid crystals in pressure-driven channel flow. J. Non-Newtonian Fluid Mech., 79 (1998), 515-527.

[4] S. Chandrasekhar, Liquid Crystals, Cambridge University Press, Chapter 3, 1977.

[5] C. Denniston, Disclination dynamics in nematic liquid crystals, Phys. Rev. B, 54 (1996), 6272-6275.

[6] M. Doi and S. F. Edwards, The Theory of Polymer Dynamics, Oxford University Press, New York, 1986.

[7] Q. Du, B. Y. Guo and J. Shen, Fourier spectral approximation to a dissipative system modeling the flow of liquid crystals, SIAM J. Numer. Anal., 39 (2001), 735-762.

[8] J. L. Ericksen, Conservation laws for liquid crystals, Trans. Soc. Rheol., 5 (1961), 23-34.

[9] J. J. Feng, J. Tao and L. G. Leal, Roll cells and disclinations in sheared nematic polymers, J. Fluid Mech., 449 (2001), 179-200.

[10] P. G. de Gennes and J. Prost, The Physics of Liquid Crystals, second edition, Oxford Science, 1993.

[11] D. Grecov and A. D. Rey, Shear-induced textural transitions in flow-aligning liquid crystal polymers, Phys. Rev. E, 68 (2003), 061704.

[12] S. Z. Hess, Fokker-Planck-equation approach to flow alignment in liquid crystals, Z. Naturforsch, 31A (1976), 1034-1037.

[13] M. Kleman, Defects in liquid crysrals, Rep. Prog. Phys., 52 (1989), 555-654.

[14] M. V. Kurik and O. D. Lavrentovich, Defects in liquid crysrals: homotopy theory and experimental studies, Sov. Phys. Usp. 31 (1988), 196-224.

[15] R. G. Larson, The Structure and Rheology of Complex Fluids, Oxford Unversity Press, 1999.

[16] F. H. Lin and C. Liu, Global existence of solutions for Ericksen-Leslie system, Arch. Rat. Mech. Anal., 154 (2001), 135-156.

[17] P. Lin and C. Liu, Simulations of singularity dynamics in liquid crystal flows: A C^0 finite element approach, J. Comput. Phys., 215 (2006), 348-362.

[18] F. H. Lin, C. Liu and P. Zhang, On hydrodynamics of viscoelastic fluids, Commun. Pure Appl. Math., 58 (2005), 1-35.

[19] P. Lin, C. Liu and H. Zhang, An energy law preserving C^0 finite element scheme for simulating the kinematic effects in liquid crystal dynamics, J. Comput. Phys., 227 (2007), 1411-1427.

[20] C. Liu, J. Shen and X. F. Yang, Dynamics of defect motion in nematic liquid crystal flow: modeling and numerical simulation, Commun. Comput. Phys., 2 (2007), 1184-1198.

[21] C. Liu and H. Sun, On energetic variational approaches in modeling the nematic liquid crystal flows, Discrete and Continuous Dynamical Systems, 23 (2009), 455-475.

[22] C. Liu and N. J. Walkington, Approximation of liquid crystal flows, SIAM J. Numer. Anal., 37 (2000), 725-741.

[23] C. Liu and N. J. Walkington, Mixed methods for the approximation of liquid crystal flows, M2AN, 36 (2002), 205-222.

[24] H. Mori, E.C. Gartland, J.R. Kelly and P.J. Bos, Multidimensional director modeling using the Q tensor representation in a liquid crystal cell and its application to the π cell with patterned electrodes, Jpn. J. Appl. Phys. 38 (1999), 135-146.

[25] N. Mottram and C. Newton, Introduction to Q-tensor theory, University of Strathclyde Mathematics, Research Report, 2004, No.10, http://www.mathstat.strath.ac.uk/people/academic/nigel-mottram

[26] V.G. Nazarenko and O.D. Lavrentovich, Archoring transition in a nematic liquid crystal composed of centrsymmetric molecules, Phys. Rev. E, 49 (1994), 990-994.

[27] G. S. Ranganath, Defects in liquid crystals, Current Science, 59 (1990), 1106-1124.

[28] A. D. Rey, Theory of linear viscoelasticity of chiral liquid crystals, Rheol Acta, 35 (1996), 400-409.

[29] A. D. Rey and M. M. Denn, Dynamical phenomena in liquid-crystalline matericals, Annu. Rev. Fluids Mech., 34 (2002), 233-266.

[30] A. D. Rey, Capillary models for liquid crystal fibers, membranes, films, and drops, Soft Matter, 3 (2007), 1349-1368.

[31] A. D. Rey and T. Tsuji, Recent advances in theoretical liquid crystal rheology, 7 (1998), 623-639.

[32] C. Satiro and F. Moraes, Lensing effects in a nematic liquid crystal with topological defects, Eur. Phys. J. E, 20 (2006), 173-178.

[33] T. Tsuji and A. D. Rey, Effect of long range order on sheared liquid crystalline materials: Part 1: compatibility between tumbling behavior and fixed anchoring, J. Non-Newtonian Fluid Mech., 73 (1997), 127-152.

[34] T. Tsuji and A. D. Rey, Orientation mode selection mechanisms for sheared nematic liquid crystalline materials, Phys. Rev. E, 57 (1998) 5609-5627.

[35] G. Toch, C. Denniston and J. M. Yeomanns, Hydrodynamics of topological defects in nematic liquid crystals, Phys. Rev. Lett., 88 (2002), 105504.

[36] Q. Wang, M. G. Forest and R. Zhou, A kinetic theory for solutions of nonhomogeneous nematic liquid crystalline polymers with density variations, J. Fluids Eng., 126 (2004), 180-188.

[37] Q. Wang, A hydrodynamic theory for solutions of nonhomogeneous nematic liquid crystalline polymers of different configurations, J. Chem. Phys., 116 (2002), 9120-9136.

[38] X. F. Yang, M. G. Forest, W. Mullins and Q. Wang, Quench sensitivity to defects and shear banding in nematic polymer film flows, J. Non-Newtonian Fluid Mech., 159 (2009), 115-129.

[39] H. Yu and P. Zhang, A kinetic-hydrodynamic simulation of microstructure of liquid crystal polymers in plane shear flow, J. Non-Newtonian Fluid Mech., 141 (2007), 116-227.

[40] H. Zhang and Q. Bai, Numerical investigation of tumbling phenomena based on a macroscopic model for hydrodynamic nematic liquid crystals, Commun. Comput. Phys., 7 (2010), 317-332.

[41] S. Zhang, C. Liu and H. Zhang, Numerical simulations of hydrodynamics of nematic liquid crystals:effects of kinematic transports, Commun. Comput. Phys., 9 (2011), 974-993.